CZECH TECHNICAL UNIVERSITY IN PRAGUE
FACULTY OF MECHANICAL ENGINEERING

BACHELOR THESIS

# Design and characterization of small solid-propellant rocket engine

Michal Málek

Prague 2019

## Declaration

I declare that I have developed and written this Bachelor thesis completely by myself, under the guidance of thesis supervisor Mgr. Jaroslav Kousal Ph.D. All sources used are declared in the list of literature.

In Prague…….. ……..

## Anotační list

| | | |
|---|---|---|
| **Jméno autora:** | Michal Málek | |
| **Název práce:** | Konstrukční návrh a charakterizace malého motoru na tuhé pohonné látky | |
| **Anglický název práce:** | Design and characterization of small solid-propellant rocket engine | |
| **Akademický rok:** | 2018/2019 | |
| **Ústav:** | Ústav letadlové techniky | |
| **Vedoucí práce:** | Mgr. Jaroslav Kousal Ph.D. | |
| **Bibliografické údaje:** | Počet stran: | 47 |
| | Počet obrázků: | 38 |
| | Počet tabulek: | 1 |
| | Počet příloh: | 5 (na CD) |

| | |
|---|---|
| **Klíčová slova:** | Raketový motor, tuhé palivo, tryska |
| **Keywords:** | Rocket motor, solid propellant, nozzle |

**Anotace:**

| | |
|---|---|
| **česky:** | Cílem této práce je navrhnout a zkonstruovat malý nízkoimpulsní raketový motor na tuhé pohonné látky a charakterizovat jeho výkonové parametry. |
| **anglicky:** | The goal of this bachelor thesis is to design and build a small solid-propellant rocket motor and to characterize its performance. |

## Acknowledgement

I would like to thank to Mgr. Jaroslav Kousal Ph.D. for his guidance and assistance during my work on this bachelor thesis and to Ing. Bohuslav Křížek for his valuable advices.

My deepest gratitude is also towards my family that has supported me not only during my work on this thesis, but throughout my entire life as well.

Last but not least I would like to thank to past and present employees of NASA, ESA, SpaceX and all other space agencies for their incredible work and overwhelming achievements which kept me fascinated about aerospace engineering.

# Table of contents

# I. Introduction

Space exploration as we know it today would not be possible to achieve without powerful rockets capable of overcoming the Earth's gravity and reaching significant speeds, to allow various spacecrafts to travel across the solar system.

If we go back in time into the history, back in 13th century, when the first gunpowder-powered rockets evolved in medieval China, their creators probably had no idea, how important their invention is, and how massive impact it will have at the turn of the millennium.

While these rockets were mostly used as inaccurate long-range military weapons and fireworks, in the last century with the fast-paced development driven by two world wars and following space race to the Moon they evolved into heavy and powerful launchers capable of sending humans into space and unmanned probes across the Solar system and beyond. It is clear, that the development of spacecraft technology over last decades greatly contributed to the technology level of today's civilisation.

# II. Theory

## 2.1. Basics

### 2.1.1. Laws of physics

Rockets are powered by a propulsion device called “rocket engine”. These engines can vary in size, performance, the type and state of the fuel, but all of them share the same principle of operation.

Rockets follow the Newton's Third Law of Motion, which states:

*"For every action there is an equal and opposite reaction."*

This means, that when the rocket engine produces force (thrust) in the direction of the nozzle, equal force is applied back at rocket in opposite direction.

This is achieved by chemical reaction of the fuel and oxidiser (collectively called “propellants”) in the combustion chamber of the engine, where they are mixed and burned at high temperature, forming hot gases which expand rapidly. These gases are then ejected at high velocity through the nozzle, creating thrust and accelerating the engine in opposite direction. *[1]*

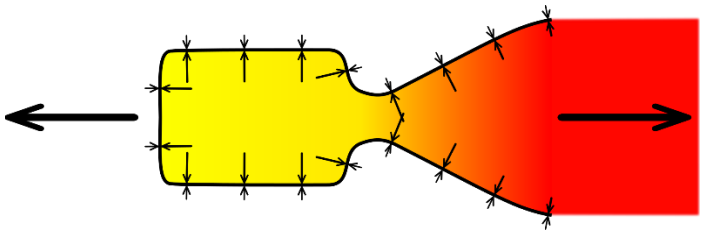

*Fig. 1 – force diagram for rocket engine [2]*

The acceleration of the rocket depends on Newton's Second Law of Motion, which states that the rate of change of momentum of a body (rocket) is directly proportional to the force applied – this change in momentum takes place in the direction of the applied force“.

This can be mathematically described as:

$$F = m\frac{dv}{dt} = ma$$

*Where:*

*F = net force applied*

*m = assumed constant mass of the rocket*

*dv/dt = change in velocity of the rocket in time*

*a = acceleration*

However, since rockets burn their fuel and therefore are considered to be variable-mass objects, it is necessary to correctly describe their motion. Correct equation for rocket behaviour therefore is:

$$F = m(t)\frac{dv}{dt} - u\frac{dm}{dt}$$

*Where:*

*m(t) = rocket mass variable in time*

*u = velocity of ejected mass* ***relative to the rocket***

*dm/dt = ejected mass in time (mass flow rate)*

### 2.1.2. Specific impulse

The specific impulse $I_{sp}$ represents the thrust per unit propellant "weight" flow rate. It is an important figure of merit of the performance of any rocket propulsion system, a concept similar to miles per gallon parameter as applied to automobiles. A higher number often indicates better performance. The specific impulse is measured in seconds. *[3]*

### 2.1.3. Tsiolkovsky equation

The Tsiolkovsky rocket equation, classical rocket equation, or ideal rocket equation is a mathematical equation that describes the motion of vehicles that follow the basic principle of a rocket: a device that can apply acceleration to itself using thrust by expelling part of its mass with high velocity can thereby move due to the conservation of momentum.

The equation relates the delta-v (the maximum change of velocity of the rocket if no other external forces act) to the effective exhaust velocity and the initial and final mass of a rocket, or other reaction engine. [4]

$$\Delta v = v_e \ln\left(\frac{m_{initial}}{m_{final}}\right)$$

## 2.2. Types of propulsion

Rockets are powered by various types of engines, each having its own advantages and disadvantages:

- **Solid-propellant rockets** are chemical rockets where the propellant is burned in a solid state. Solid-propellant motors are relatively cheap to build, maintain and operate. They are very reliable and produce significant amount of thrust. The downside is, once ignited they cannot be shut down and it is not possible to control their thrust. They also have worse specific impulse than standard liquid propellant engines.

  They are mostly used as first-stage boosters to improve the rocket performance early in the flight. For example the SRBs of Ariane 5 rocket produce up to 90% of total thrust at the liftoff.

- **Liquid-propellant rockets** have liquid fuel and oxidizer stored in separate tanks. These two ingredients are then fed into the combustion chamber via pumps, where they burn in a specific mixture ratio. Liquid-propellant engines are quite complex, but their thrust can be reduced to some extent and they can be shut down at any time and in some cases even reignited. They utilize wide range of fuels, such as Hydrogen, Kerosene (RP-1) or Hydrazine.

  Liquid propellant engines are the most common type of spacecraft propulsion, therefore they are used in wide variety of applications.

- **Hybrid rockets** have stored the solid propellant in the combustion chamber, to which a second propellant in form of liquid or gas (usually the oxidiser) is added to start the combustion. Hybrid rockets avoid common disadvantages of solid and liquid rockets (such as propellant handling and mechanical complexity). However they come with own problems such as non-optimal mixing of ingredients in different states of matter. Another disadvantage is, that they have to leave part of solid fuel unburned, to avoid its disintegration and jamming the nozzle.

- **Monopropellant rockets** use a single chemical as its propellant, which is decomposed by a catalyst. The most common monopropellant is hydrazine. Monopropellant engines are simple in concept, but the $I_{sp}$ is significantly worse compared to liquid engines.

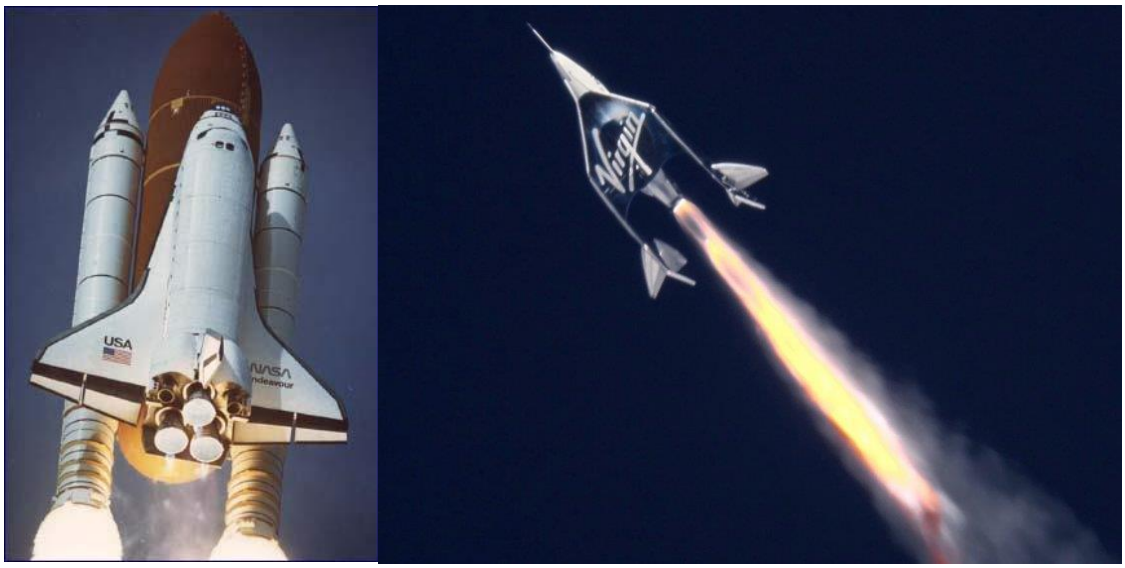


*Fig. 2 - NASA's Space Shuttle Endeavour with 2 solid-propellant boosters and 3 RS-25 liquid hydrogen/oxygen engines [5] (On the left) and Virgin Galactic's SpaceShipTwo with single hydroxyl-terminated polybutadiene (HTPB) hybrid rocket engine [6] (On the right)*

### Alternative propulsion systems

Exothermic chemical reaction is not the only way to achieve the spacecraft propulsion. The energy required can be obtained from external source, like ion engines, resistojets, or pulsed plasma thrusters.

## 2.3. Nozzle

With the exception for some experimental projects, all rockets use a **de Laval nozzle** (which is also known as **convergent-divergent nozzle**) - a tube whose cross-section area decreases in the middle and then expands again. The hot, pressurized gas is accelerated passing through the throat of the nozzle to a higher supersonic speed in the axial direction, by converting the heat energy of the flow into kinetic energy. As the gas travels through the nozzle, its pressure and temperature decrease. Meanwhile the speed fluently increases from subsonic to sonic at the throat and furthermore to supersonic speed in the divergent section of the nozzle as seen in Fig. 4.

In the ideal case of maximal efficiency, the gas pressure at the exit of the nozzle equals the ambient pressure. (see Fig. 1 and Fig. 3)

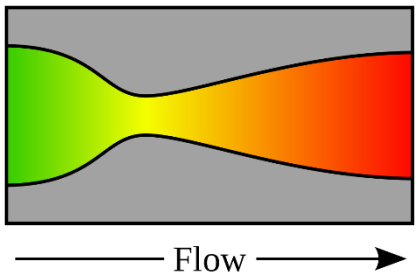


*Fig. 3 - Example of de Laval nozzle, showing the flow velocity increasing from green to red in the direction of flow [7]*

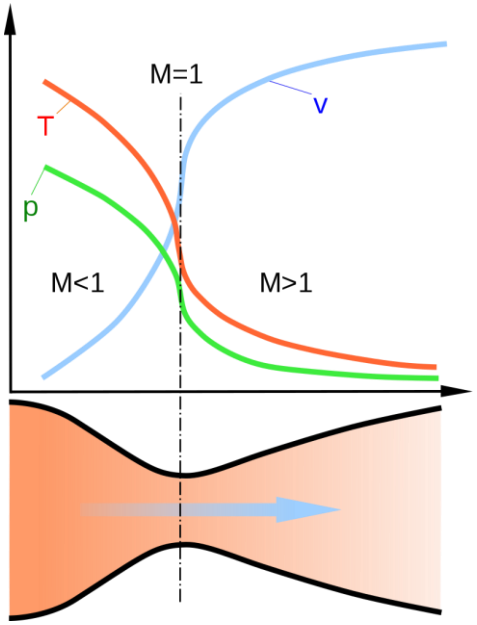


*Fig. 4 - Diagram of a De Laval nozzle [8]*

*where:*

*v = flow velocity*

*T = temperature*

*p = pressure*

The linear velocity of the exhaust gases exiting the nozzle can be calculated using the following equation:

$$v_e = \sqrt{\frac{TR}{M} \cdot \frac{2\gamma}{\gamma - 1} \cdot \left[1 - \left(\frac{p_e}{p}\right)^{\frac{\gamma-1}{\gamma}}\right]}$$

*Eq. 1 – gas velocity*

*Where:*

$v_e$ *= exhaust velocity at the nozzle exit*

*T = absolute temperature of inlet gas*

*R = universal gas law constant (8314.5 J/kmol·K)*

*M = molecular mass of the gas*

*γ =* $c_p/c_v$ *= isentropic expansion factor*

$c_p$ *= specific heat of the gas at constant pressure*

$c_v$ *= specific heat of the gas at constant volume*

$p_e$ *= absolute pressure of the exhaust gas at the exit of the nozzle*

*p = absolute pressure of the inlet gas*

The nozzle shape and size is very important, as it directly affects the efficiency. Bell-shaped nozzles are the most common as they can be shorter and lighter than simple cone-shaped ones. They are slightly more efficient as well (approximately 1% difference). However they are more complex, harder to manufacture and therefore cost more.

Apart from these two examples, there are advanced nozzle designs such as aerospike or stepped (dual-bell) nozzles. These bring new advantages and challenges, but aren't widely used.

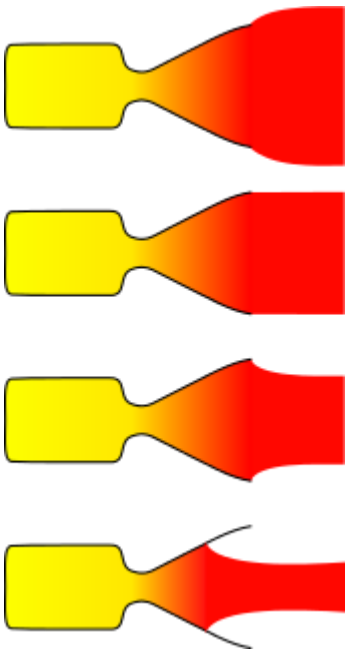

- **under-expanded** (exit pressure is greater than ambient pressure)
- **perfectly expanded** (exit pressure equals ambient pressure)
- **over-expanded** (exit pressure is smaller than ambient pressure)
- **grossly over-expanded** (same problem as over-expanded, but with a shock wave forming inside the nozzle extension)

*Fig. 5 - Different scenarios of nozzle expansion [9]*

## 2.4. Deeper understanding of solid-propellant motors

### 2.4.1. History of solid propellant rockets

The first gunpowder-powered rockets may have appeared as early as in 10$^{th}$ century in ancient China, however any solid documentary evidence does not appear until the 13$^{th}$ century under the dynasty of Songs. These primitive rockets attached to arrows were initially used as a long-range military weapon and intimidatory fireworks. Later they were adopted by Mongols and quickly spread over whole Eurasia via the Mongol invasion.

### 2.4.2. Advantages of solid propellant

Solid propellant rockets produce a lot of thrust, are very easy to store and handle compared to liquid propellant rockets. Higher fuel density allows more compact designs and in general they are the cheapest option of the rocket propulsion available. Solid propellant motors are characteristic for many past, present and future rockets, such as Delta II, Space Shuttle, Atlas V, Ariane VI or Vega-C.

### 2.4.3. Disadvantages of solid propellant

The most constraining disadvantage of a solid propellant motor is the inability to be throttled in real time (this can be partially overcome by adjusting the internal geometry of the propellant grain – see chapter 2.4.5.). For this reason, solid fuel motors are only used as first stage boosters (with exception of European Vega-C rocket, which utilizes solid fuel motors in first three of its four stages). Another drawback is significantly worse specific impulse compared to liquid engines.
Cracks and voids in the fuel grain introduce a serious hazard as they can cause unexpected increase of the burning area, locally raising the temperature and pressure, potentially leading to critical failure and loss of spacecraft.

### 2.4.4. Solid-propellant grain geometry

Because the thrust is directly related to the instantaneous burning area, the performance of solid-propellant motors cannot be managed on the fly. Instead, it is pre-determined by the shape of the propellant grain in the combustion chamber. Various shapes were designed to affect the thrust curve and deliver the required performance (as seen in Fig. 6)

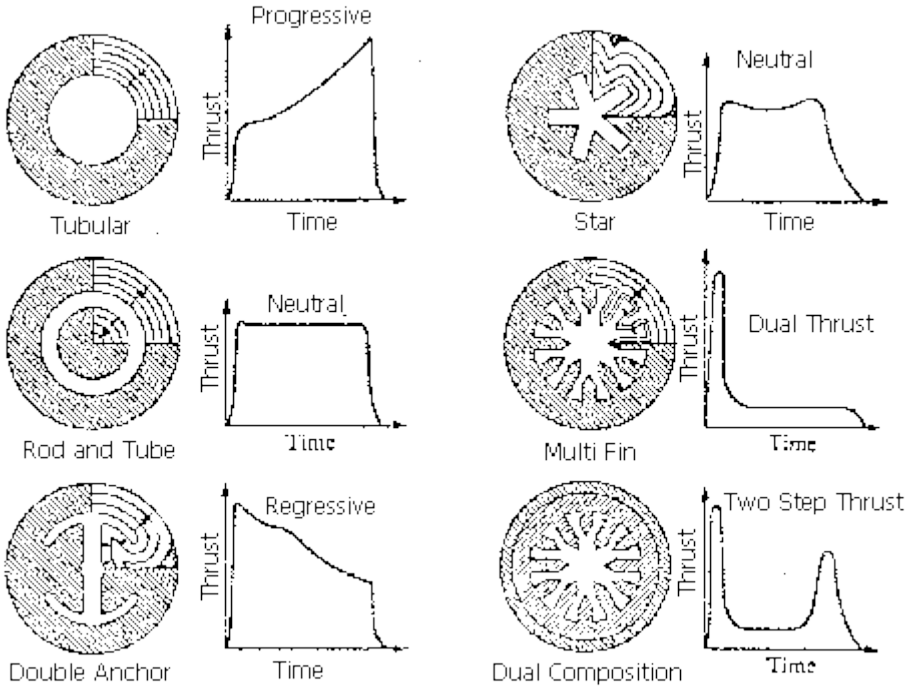


*Fig. 6 - Different grain geometries and their effect on the performance [10]*

### 2.4.5. Advanced fuel geometry design

Advanced solid-fuel engines use fuel grain geometry called "BATES" (which is an acronym for BAllistic Test and Evaluation System). This specific design has a cylindrical shape, where the outer surface is inhibited as usual, but ends of the grain are free to burn. This brings two major advantages. It allows the propellant to be divided into smaller identical sections, making the manufacturing and assembly process easier. More importantly, when a specific ratio between the outer diameter and segment length is reached (close to 1:1,7) the total size of the burning area is very consistent as the fuel burns down, resulting in very steady thrust curve. This happens, because as the inner cylindrical surface is significantly expanding over time, the area of two end surfaces is getting smaller and the overall length of the grain is being reduced as well.

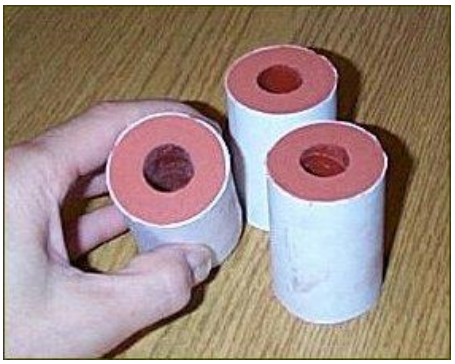

*Fig. 7 - Example of BATES propellant grain geometry [11]*

### 2.4.6. Solid propellants

Solid propellants are wide used for its simplicity and easy handling. Apart from first stage boosters, they are essential part of amateur and experimental rocketry. There are several types of compounds available.

- **Black powder (gunpowder) propellant** - One of the oldest pyrotechnic compositions. Consists of charcoal, potassium nitrate and sulfur. It is cheap and very easy to produce, therefore it is very popular choice within model rocket motor. The $I_{sp}$ of black powder is rather low (around 80 seconds) and as the fuel grain is sensitive to cracks, therefore it is typically only used in weak motors with thrust under 40 newtons.
- **Zinc-sulfur propellant** - Consists of powdered zinc mixed with powdered sulfur. It has poor performance and therefore it does not find any practical use outside amateur model rocketry.
- **"Candy" propellant** - Moulded mixture of potassium nitrate and sugar fuel (mostly sorbitol, but dextrose and sucrose are also typical). Fairly easy to produce and maintain. This kind of propellant generates $I_{sp}$ of around 130 s, making it a good candidate for amateur and experimental rocketry.
- **Composite propellants** – Mixture of powdered oxidiser with powdered metal fuel and rubbery binder. They are often either ammonium nitrate-based (ANCP), or ammonium perchlorate-based (APCP). ANCP propellants often use magnesium and/or aluminium as the fuel - they deliver medium performance ($I_{sp}$ of about 210 s), while APCP propellants use only aluminium and deliver rather high performance ($I_{sp}$ of nearly 300 s). APCP is widely used in space rockets, military rockets, as well as amateur and hobby rockets.

  APCP was also used in Space Shuttle Solid Rocket Boosters. The propellant mixture in each SRB motor consists of an ammonium perchlorate (oxidizer, 69.6 percent by weight), aluminum (fuel, 16 percent), iron oxide (a catalyst, 0.4 percent), a polymer (a binder that holds the mixture together, 12.04 percent), and an epoxy curing agent (1.96 percent). The propellant is an 11-point star-shaped perforation in the forward motor segment and a double-truncated-cone perforation in each of the aft segments and aft closure. [12]

# III. Experimental part

## 3.1. Introduction

In this part of thesis a brief summary of the chamber and nozzle development will be presented, followed by strength analysis of critical spots of the device. A brief look at the manufacturing process will be introduced before a significant attention will be paid to the main static test of the motor, its results and consequences.

## 3.2. Development

The development began with researching of available materials. As the aim was to build a relatively cheap rocket motor, the research was centered mainly on pre-fabricated materials to minimise manufacturing costs. Results of this research greatly affected the proposed dimensions of the motor. The main bottleneck were available PVC tubes, which were supposed to be used as propellant inhibitors and thermal isolation.

As I had no practical experience with development of experimental rocket motors, I was unsure how to develop the device properly. Luckily the Richard Nakka's Experimental Rocketry Web Site offered a very useful Excel sheet, which provided a lot of insight on the development of experimental propulsion systems and guided me in the process. [13]

*The attached .xls file contains the exact values used in the development of this rocket motor.*

### 3.2.1. The fuel and chamber geometry

Development began with determining what kind of fuel will be used for this project. I chose the “KNSB” propellant mixture consisting of 65% of $KNO_3$ and 35% of sorbitol. This mixture is also known as “Candy” propellant and is widely used in amateur experimental rocketry - it is proven to be safe, reliable and easy to produce and maintain. It burns at approximately 1600°C and has $I_{sp}$ of about 130 s.

Next the combustion chamber dimensions were to be decided. Based on the pre-fabricated materials available, the diameter of the chamber was chosen.

$D_c = 36\,mm$

The chamber length $L_c$ was still open at this point. Next step was to determine the propellant grain geometry. After extensive trial and error activity in the Excel sheet, a decent BATES propellant grain geometry was discovered.

$D = 36\ mm$ (inhibited outer diameter)
$d_o = 15\ mm$ (exposed core diameter)
$L_o = 50\ mm$ (segment length)
$n = 2$ (number of grains in the chamber)

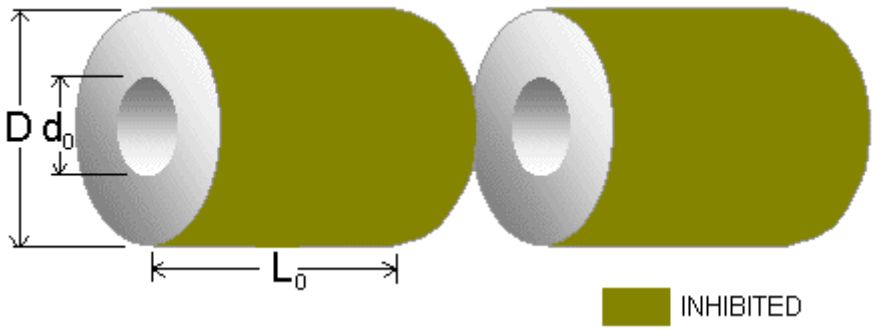


*Fig. 8 – the typical BATES geometry [10]*

This geometry would secure a very steady burning area and thus stable performance.

$V_{propellant_{initial}} = 84166\ mm^2$ (initial propellant volume)
$\rho_{propellant} = 1{,}731 \frac{g}{cm^3}$ (estimated propellant density)
$m_{propellant} = 0{,}146\ kg$ (expected propellant mass)

At this point with known grain length and the amount of grains it was possible to calculate the necessary chamber length. With extra space for burning of exposed grain ends, 110 mm was sufficient.

$L_c = 110\ mm$

Following step was to determine the desired working pressure. I was quite careful and went for relatively safe low target pressure value of 2 MPa (which later turned out to be way too cautious but I decided to stick with it).

$p = 2\ MPa$

Based on the selected chamber pressure and proposed propellant geometry, the KN value (maximal burning area / throat area ratio) was determined to be 166 (see Fig. 9).

$KN = 166$

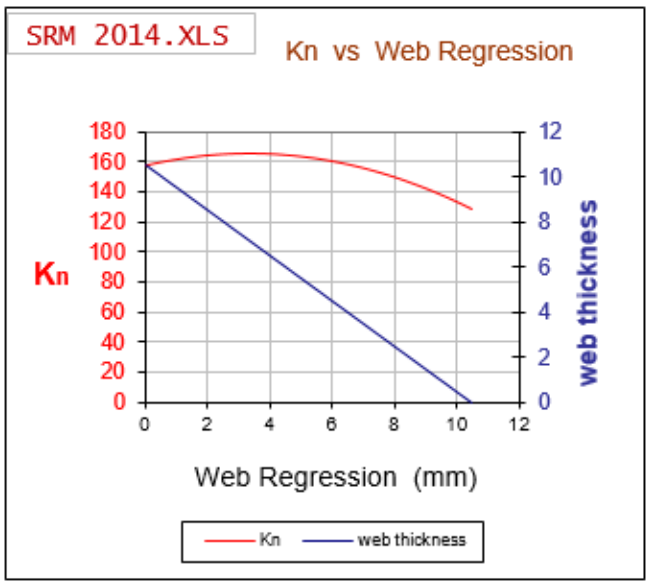


*Fig. 9 – evolution of burning area/throat area ratio over time*

With known maximal burning area $A_{b_{max}}$ and KN ratio values, it was easy to calculate the throat cross-section area and the throat diameter:

$$A_t = \frac{A_{b_{max}}}{KN} = \frac{8496}{166} = 51{,}18\ mm^2$$

$$D_t = \sqrt{4A_t/\pi} = 8{,}08\ mm$$

### 3.2.2. Nozzle geometry

Next step was to determine the nozzle expansion ratio and its exit size.

$$\frac{A^*}{A_e} = \left(\frac{k+1}{2}\right)^{k-1} \left(\frac{P_e}{P_o}\right)^{\frac{1}{k}} \sqrt{\frac{(k+1)}{(k-1)}\left[1 - \left(\frac{P_e}{P_o}\right)^{\frac{k-1}{k}}\right]}$$

$$\frac{A_e}{A^*} = 4{,}327$$

Where:

$k = 1{,}042$ (ratio of specific heats)

$P_e = 101000$ Pa (nozzle exit pressure (ambient pressure))

$P_o = 2000000\ Pa$ (chamber pressure)

$\frac{A_e}{A^*}$ is the desired ideal expansion ratio

The optimal expansion ratio is 4,327; for further calculations the expansion ratio of 4,5 was used instead.

$$A_e = 4{,}5 \cdot A_t = 230{,}8\ mm^2$$

$$D_e = \sqrt{4A_e/\pi} = 17{,}14\ mm$$

For the nozzle geometry, the most common half-angle values were used to maintain usual efficiency.

$\propto = 12°$

$\beta = 30°$

**Nozzle Design**

| | | | | |
|---|---|---|---|---|
| beta | 30,0 | degrees | Nozzle convergence half-angle | |
| alpha | 12,0 | degrees | Nozzle divergence half-angle | |
| | | | | *Reference worksheets:* |
| Dc | 36 | mm | Chamber inside diameter | *Data and Kn* |
| Dt | 8,08 | mm | Nozzle throat diameter | *Data and Kn* |
| De | 17,14 | mm | Nozzle exit diameter | *Performance* |
| De opt | 16,81 | mm | Optimum nozzle exit diameter | *Performance* |
| **Lc** | **24,18** | mm | **Convergence length** | |
| **Ld** | **21,31** | mm | **Divergence length** | |
| **Lo** | **45,49** | mm | **Overall length** | |

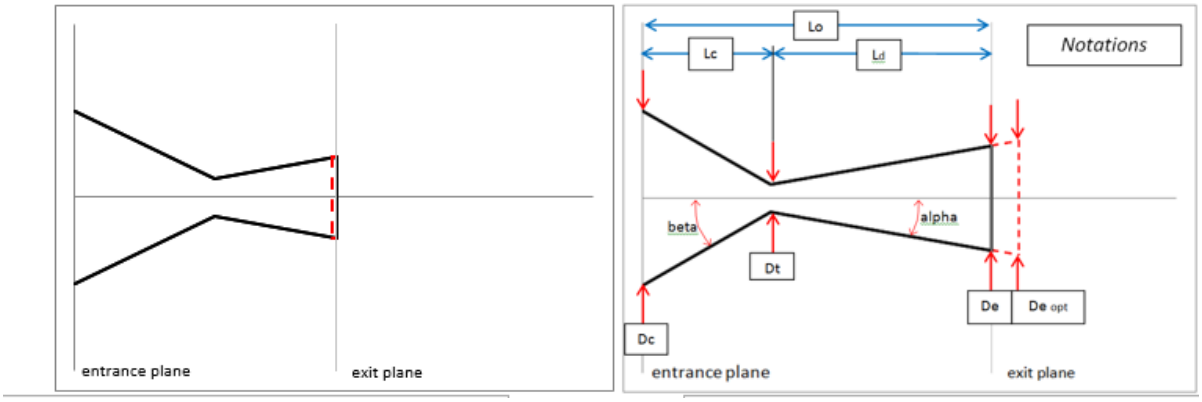


*Fig. 10 – nozzle geometry*

The length of the throat section was increased to stabilise the flow and maintain round numbers for manufacturing purposes.

### 3.2.3. Thrust prediction

The classic thrust equation was applied to every point of the burn to create the expected thrust curve as seen in Fig. 11.

$$F = I_{sp}\left(\frac{dm}{dt}\right)g$$

Where:

$I_{sp} = 110{,}3\ s$ (specific impulse)

$\frac{dm}{dt}$ (change of mass in time)

$g = 9{,}81\ m/s^2$ (standard gravitational constant)

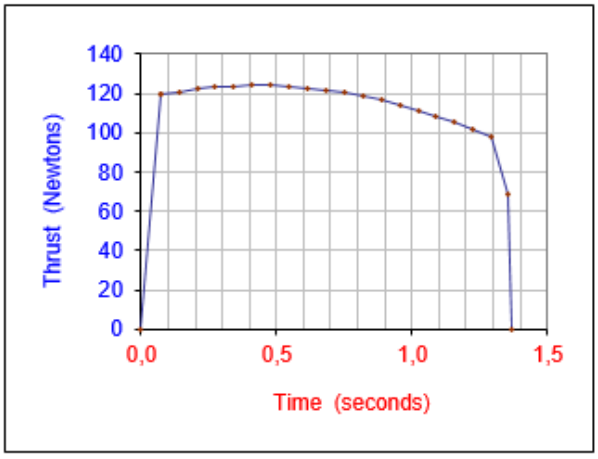


*Fig. 11 – Expected thrust curve*

### 3.2.4. Construction concept

I was evaluating a lot of possible concepts of the motor construction. In the discussion with Ing. Bohuslav Křížek I was recommended to avoid overengineering and to stick to simplest design possible. In the end I went for aluminium casing with a retaining ring at each end of the hole. This design is very simple and in case of critical event it allows the motor to fail safely by releasing the energy in the direction of the main axis.

### 3.2.5. The CAD model

The motor itself was designed in Autodesk Inventor 2017. In Fig. 13 all dimensions are in millimetres.

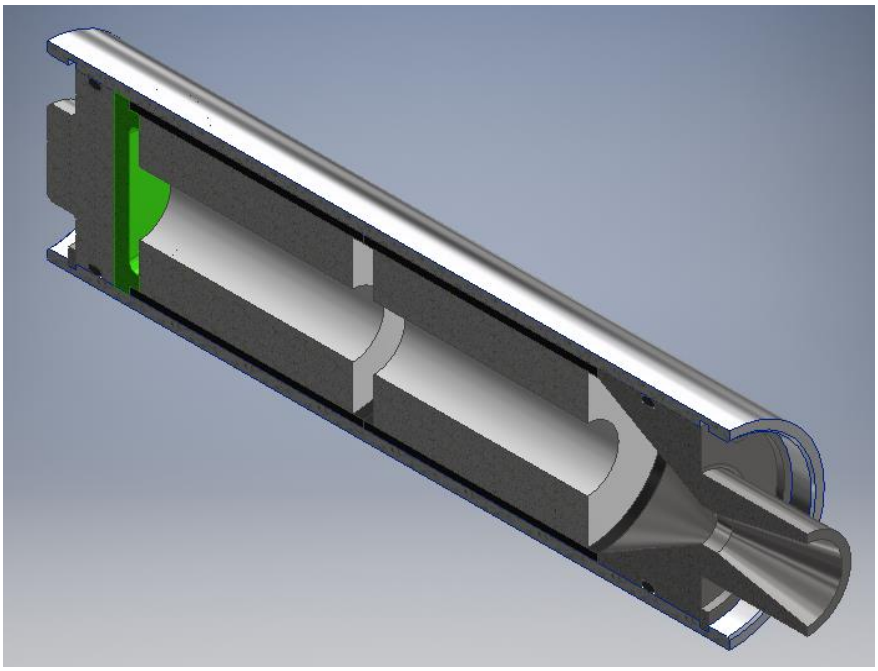

*Fig. 12 – 3D CAD model cut in half*

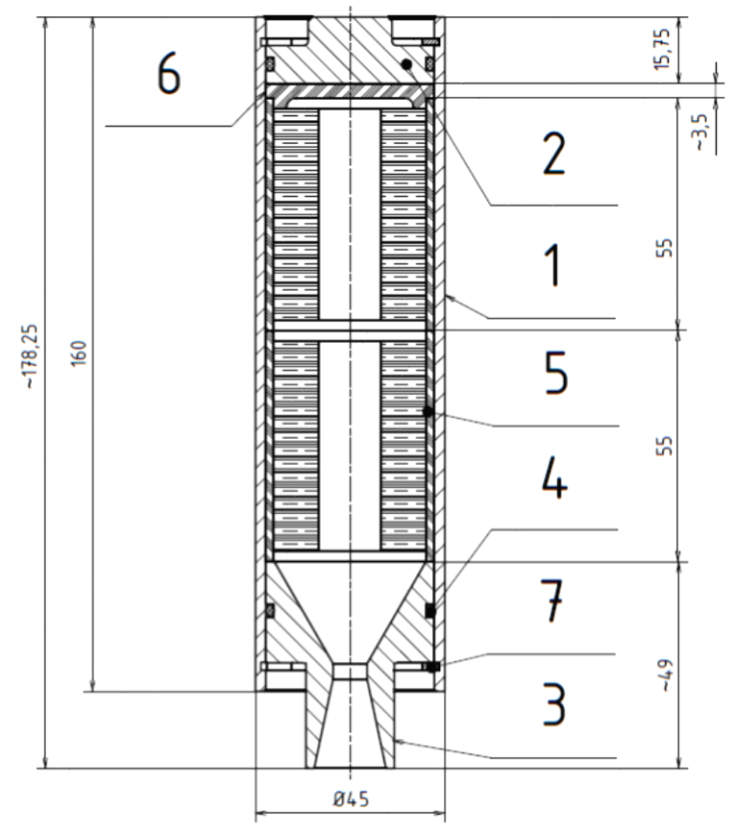


*Fig. 13 – Proposed motor assembly*

1 – aluminium casing
2 – aluminium cover
3 – stainless steel nozzle
4 – sealing rings (2x)
5 – PVC inhibitor with KNSB propellant (2x)
6 – 3D-printed stopper
7 – retaining rings (2x)

### 3.2.6. Stress-check at critical spots

### 3.2.6.1. Casing verification – thick pressure vessel

Input data:

$r_1$ = 40 mm (inner radius)

$r_2$ = 45 mm (outer radius)

$p_1$ = 2 MPa (inside pressure)

$p_2$ = 0,1 MPa (outside (ambient) pressure)

$\sigma_D$ = 200 MPa (allowed stress)

Equations:

$$\sigma_a = K = \frac{p_1 {r_1}^2 - p_2 {r_2}^2}{{r_2}^2 - {r_1}^2} = 7{,}053\ N/mm^2$$

$$\sigma_{r_{(r_1)}} = -p_1 = -2\ N/mm^2$$

$$\sigma_{t_{(r_1)}} = 2K + p_1 = 16{,}1\ N/mm^2$$

$$\sigma_{r_{(r_2)}} = -p_2 = -0{,}1\ N/mm^2$$

$$\sigma_{t_{(r_2)}} = 2K + p_2 = 14{,}21\ N/mm^2$$

$$\sigma_{red} = \sigma_{t_{(r_1)}} - \sigma_{r_{(r_1)}} = 18{,}1\ N/mm^2 \leq \sigma_D$$

$$k = \frac{\sigma_D}{\sigma_{red}} = 11{,}05$$

Results:

$\sigma_a$ = 7,053 $N/mm^2$ (axial stress)

$\sigma_{r_{(r_1)}}$ = -2 $N/mm^2$ (radial stress at $r_1$)

$\sigma_{t_{(r_1)}}$ = 16,1 $N/mm^2$ (tangential stress at $r_1$)

$\sigma_{r_{(r_2)}}$ = -0,1 $N/mm^2$ (radial stress at $r_2$)

$\sigma_{t_{(r_2)}}$ = 14,21 $N/mm^2$ (tangential stress at $r_2$)

$\sigma_{red}$ = 18,1 $N/mm^2$ (reduced stress)

k = 11,05 (safety coefficient)

The safety coefficient is greater than 11 – the aluminium casing meets the mechanical requirements with significant reserve.

### 3.2.6.2. Casing verification – tensile strength

Input data:

$r_1$ = 42,5 mm (inner radius at the retaining ring plane)

$r_2$ = 45 mm (outer radius)

$p$ = 2 MPa (pressure inside the chamber)

$\sigma_D$ = 200 MPa (allowed stress)

First thing is to convert the pressure to proportional force applied to the retaining ring.

$$S_{chamber} = \pi {r_1}^2 = 5674{,}5\ mm^2$$

$$F = S_{chamber} \cdot p = 11349\ N$$

The force F is then applied via retaining ring to the aluminium casing at its critical cross-sectional area.

$$S_{critical} = \pi {r_2}^2 - \pi {r_1}^2 = 687{,}22\ mm^2$$

$$\sigma = \frac{F}{S} = 16{,}51\ MPa \leq \sigma_D$$

$$k = \frac{\sigma_D}{\sigma} = 12{,}11$$

Results:

$S_{chamber}$ = 5674,5 $mm^2$ (cross-sectional area of the chamber)

$F$ = 11349 $N$ (force in the axial direction)

$S_{critical}$= 687,22 $mm^2$ (critical cross-sectional area)

k = 12,11 (safety coefficient)

The safety coefficient is greater than 12 - the stress at the critical cross-sectional area is within allowed values with great reserve.

### 3.2.6.3. Retaining rings verification – shear stress

Input data:

$F$ = 11349 $N$ (force in the axial direction)

t = 1,75 mm (retaining ring thickness)

$r$ = 40 mm (chamber radius)

$\sigma_D$ = 380 MPa (allowed stress)

From the previous part we know the force generated by the pressure in the combustion chamber.

$$F = S_{chamber} \cdot p = 11349\ N$$

The force F is then applied to adequate cross-sectional area of the retaining ring. *Note: The retaining ring does seize only about 90% of the perimeter of the hole, this fact has to be considered in the calculation.*

$$o = 2\pi r \cong 267\ mm$$

$$o_{red} = o \cdot 0{,}9 = 240{,}3\ mm^2$$

$$S = o_{red} \cdot t = 420{,}525\ mm^2$$

$$\tau = \frac{F}{S} = 26{,}99\ MPa \leq \tau_D$$

$$k = \frac{\tau_D}{\tau} = 14{,}08$$

Results:

$o$ = 267 $mm$ (perimeter of the chamber)

$o_{red} = 240{,}3\ mm$ (reduced perimeter)

$S$ = 420,525 $mm^2$ (cross-sectional area of the retaining ring)

k = 14,08 (safety coefficient)

The safety coefficient is greater than 14 - the shear stress at the critical cross-sectional area of the retaining ring is within allowed values with great reserve.

**All critical spots have been checked and are complying with the maximal allowed stress.**

### 3.2.7. Propellant test

After the motor design was mathematically validated, it was time to determine the structure of the propellant.

Although the propellant mixture consisting of 65% of $KNO_3$ and 35% of sorbitol was intended to be used since the very beginning, the consistency of the mixture and its overall manufacturing process was unclear. Two options were available and a test had to be performed to determine, which type of grain will deliver better performance.

First option consisted of a finely milled mixture of both $KNO_3$ and Sorbitol compressed by high force directly into the inhibitor. This would remove the potentially hazardous process of melting the mixture, but it would also mean less uniform mixture and questionable propellant integrity.

Second option was the traditional one – finely milled $KNO_3$ mixed with standard sorbitol grains melted in the pan and then casted into the inhibitor. This would secure more uniform propellant mixture at the cost of additional casting.

*Fig. 14 – Comparison of two propellant grains with different manufacturing process. Compressed mixture on the left, casted mixture on the right.*

Both tests were conducted in the home fire pit in similar conditions. The inhibitor with the fuel grain was put on a wooden plank in the middle. Then the standard model rocket igniter was plugged into the grain and connected to the AA battery on one side. With the use of long steel rod, the second end of the igniter cable was connected to the other side of the battery, which immediately activated the igniter and set the fuel on fire.

After both tests were performed, the difference between these mixtures was clearly visible. The compressed mixture produced huge flame and significant amount of rather dark smoke. Meanwhile the casted mixture created very little flame but huge amount of strong white smoke. The burn rate of both propellants was quite comparable, however the casted grain produced way more smoke and hot gases than its compressed counterpart.

This test proved the casted grain to be more suitable for this experimental rocket motor.

### 3.3. Manufacturing and assembly

The manufacturing process was pretty straight-forward. Aluminium casing, aluminium cover and stainless steel nozzle were manufactured via turning, the plastic stopper was printed on the lent 3D printer and inhibitors with propellant grains were made out in university workshops. The retaining rings and sealing rings were bought in local specialised shops.

Materials used:
*Aluminium: EN AW 6060*
*Stainless steel: 1.4301*
*3D-printing filament: PVA*

*Fig. 15 – All components altogether (except the 3D-printed stopper)*

*Fig. 16 – Finished BATES propellant grains.*

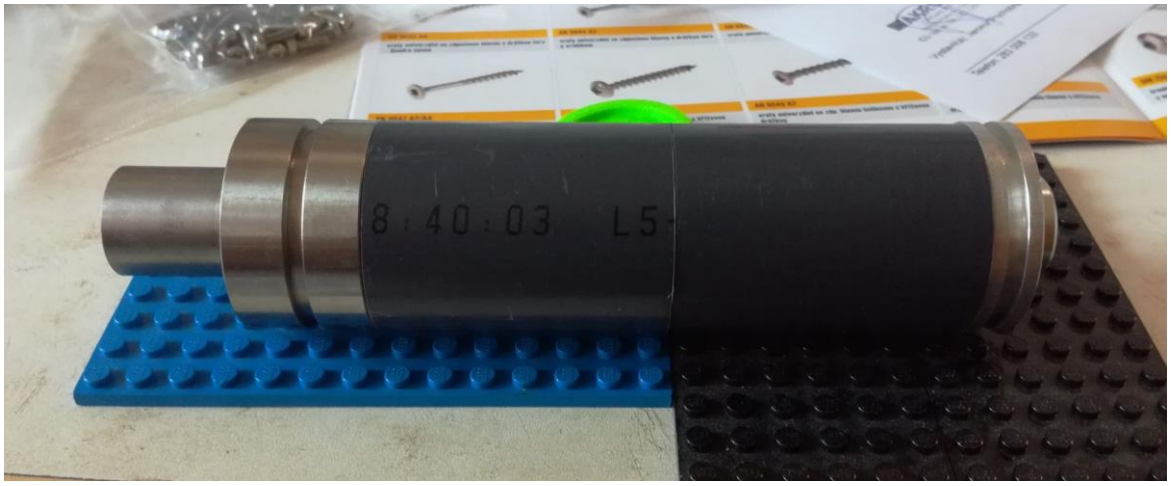


*Fig. 17 – "Pre-assembled" motor*

## 3.4. The test

### 3.4.1. Measuring apparatus

For the thrust measurement the existing apparatus was used. This apparatus was originally used in the “DRoP SlaM” project (Demonstrator of Rocket Powered Soft Landing Module – reference not available as the project documents have not yet been published) and seemed perfect for this experiment as well.

*Fig. 18 – The apparatus with mounted experimental motor*

The measuring probe was calibrated with 50N test weight, a possible relative error of 2% was conceded.

*Fig. 19 – Experimental rocket motor mounted to the measuring apparatus*

### 3.4.2. The main test

*For better understanding of the data presented in following chapters I strongly recommend to firstly watch videos from the main test. These videos can be found in the CD attached at the back of this thesis.*

The main test took place on 17th July 2019 at the court of CTU in Prague at Charles' Square. The test was initially intended to happen around 6 PM local time (to avoid the time when the court is crowded), but due to hardware and software issues the testing sequence was initialised much later around 7:15 PM. The test itself was very noisy and discharged a lot of smoke high into the air. The motor survived intact and the measured data were successfully retrieved.

*Fig. 20 – Two recorded camera views from the main test*

*Fig. 21 – T+0s (ignition)*

*Fig. 22 – T+1,0s (the pressure builds up)*

*Fig. 23 – T+1,95s (wires fly out of the nozzle as the thrust abruptly increases)*

*Fig. 24 – T+2,7s – the peak thrust with possible glimpse of Mach diamond effect*

*Fig. 25 – T+4,1s (burnout)*

### *3.5. Test aftermath and data evaluation*

*Fig. 26 – Immediate condition of the nozzle directly after the test*

### 3.5.1. Results

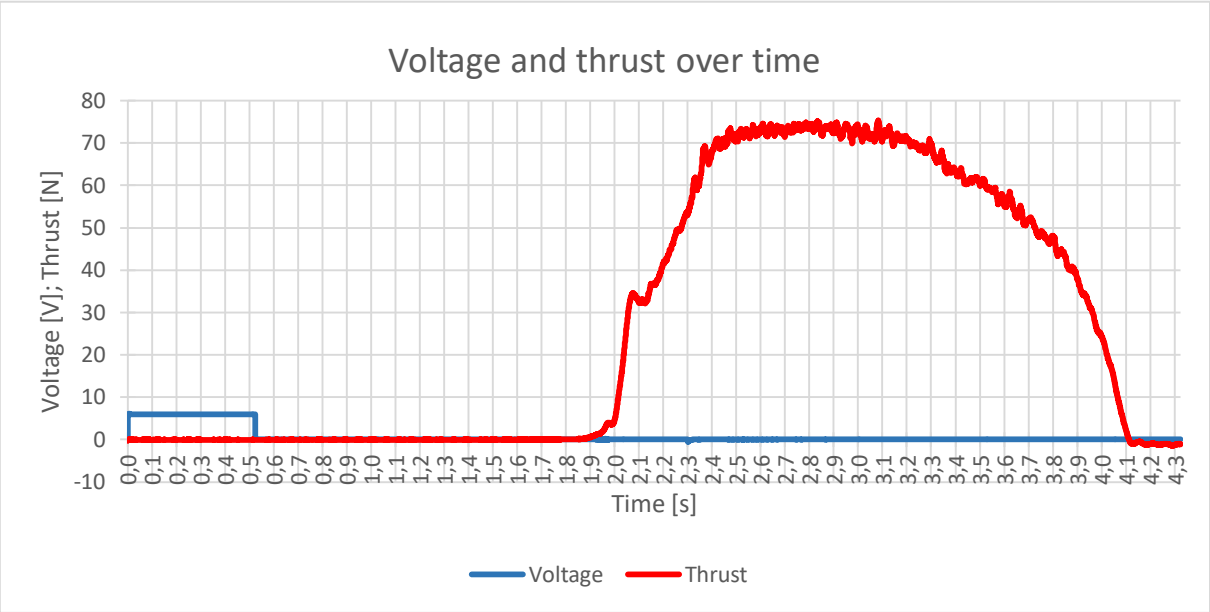


*Fig. 27 - Diagram of voltage applied at the igniter and trust measured during the main test. For better orientation each rectangle in the grid represents 1Ns of the total impulse.*

In the graph, two things immediately caught my eye. First thing being the fact, that after the ignition at T-0 it took the motor almost two seconds before it started to produce any thrust. Second interesting thing is a weird fluctuation at the thrust curve at T+2,1s.

The first phenomena can be explained quite easily – the igniter was put very deep into the combustion chamber (the re-measurement of burned wires stated the depth of about 15cm – it is safe to assume the igniter was placed at the very bottom of the chamber) and very likely not in direct contact with the propellant grain. Due to that, when the igniter was activated, the propellant failed to inflame immediately. Instead a small local fire occurred at the bottom of the chamber, further heating the propellant mixture until it fully ignited on its own nearly two seconds later.

The second phenomena is more difficult to understand. Initially I thought, that the jump in the force applied to the measuring probe was a direct result of wires being spitted out of the nozzle, creating this weird pulse at the stand. However, after carefully analysing the recorded slow-motion video synchronised with measured data, I can declare this idea to be false - wires left the nozzle at T+1,95s, while the questionable event happened at T+2,1s. Also there were no fluctuations in the stream of hot gases

coming from the nozzle at all. The temporary halt in the downward movement of the apparatus arm is noticeable in the video, however there is no clear visible cause of this issue (friction in the apparatus can be discarded as well). At this point I assume, that the thrust produced by the motor was raising steadily, and the fluctuation in the measured data at T+2,1s was caused by some unidentified external force.

I forgot to check the weight of propellant grains prior the test, however the weight difference between the new and used motor was 134,3 g (567,6 g for new and 433,3 g for used one). That is slightly less than pre-calculated 146 g, but this is not a representative value since a lot of cinder was still inside when the weight measurement was performed. Taking this (and possible small density difference) into consideration, it is reasonable to assume that the grain weight was close to its expected value.

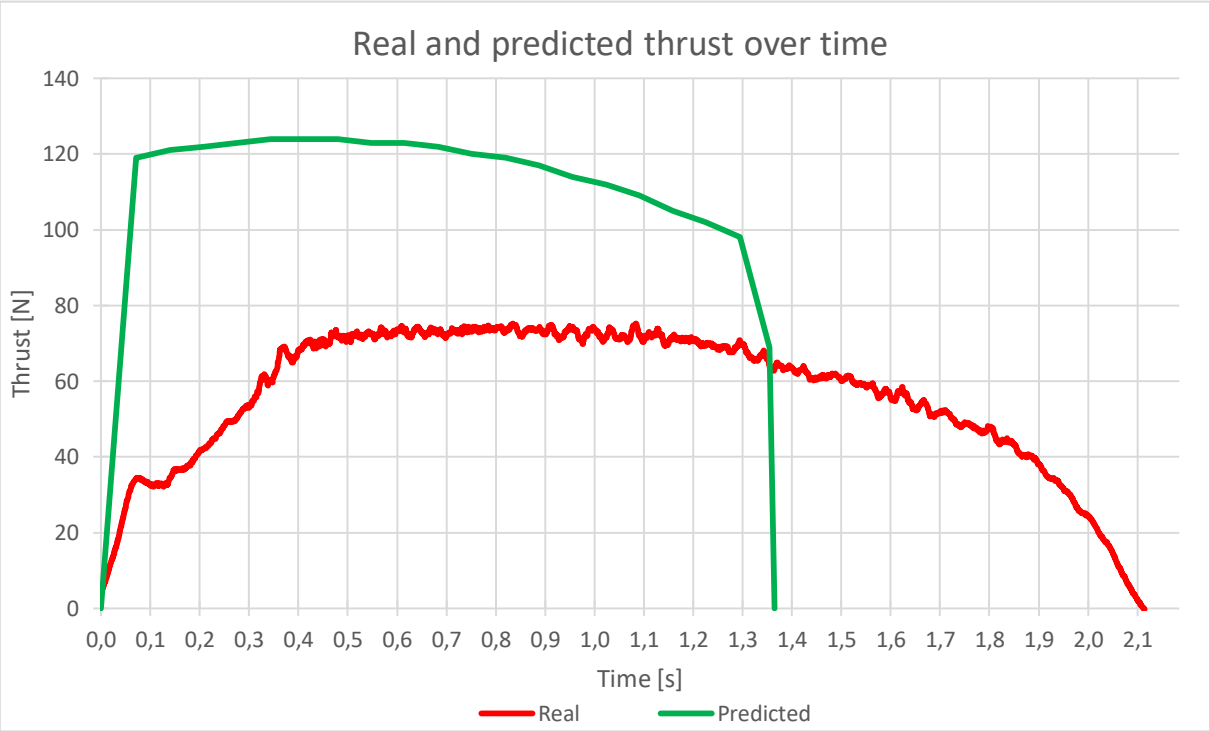


*Fig. 28 – comparison of real and predicted thrust curve*

Comparing the measured and predicted data, it is clear, that the thrust intensity was significantly lower. However, as the propellant burned for longer, the total impulse (are under the curve) is quite comparable with the prediction. Clearly the propellant burn rate was way smaller than its mathematical model used in the simulation, therefore the difference in both curves.

In fact, these two curves are directly comparable - if we apply the measured burn time to the original thrust equation (see 2.1.1.), then:

$I_{sp} = 110{,}3\ s$

$dm = 140\ g$ (approx.)

$dt = 2\ s$

$g = 9{,}81\ m/s^2$

$$F = I_{sp}\left(\frac{dm}{dt}\right)g = 75{,}8N$$

Which is exactly the peak thrust value measured in the test.

### 3.6. Disassembly and part inspection

After the test, the solid propellant motor was disassembled and all its parts were inspected. A lot of cinder was left inside, so the disassembly process was very messy. In general the motor was in way better condition than expected. Each part was cleaned and inspected for damages.

*Fig. 29 – The damaged plastic stopper still connected to the PVC inhibitor*

*Fig. 30 – Convergent section of the nozzle covered with thin layer of ash*

### 3.6.1. Part review

(in no particular order)

#### 3.6.1.1. Retaining rings

*Fig. 30 – Retaining rings*

These two rings were placed on each end of the motor to keep it together. They were not in direct contact with the heat and did not suffer any mechanical nor cosmetic damage.

Verdict: Perfect condition, suitable for reuse.

### 3.6.1.2. Cover

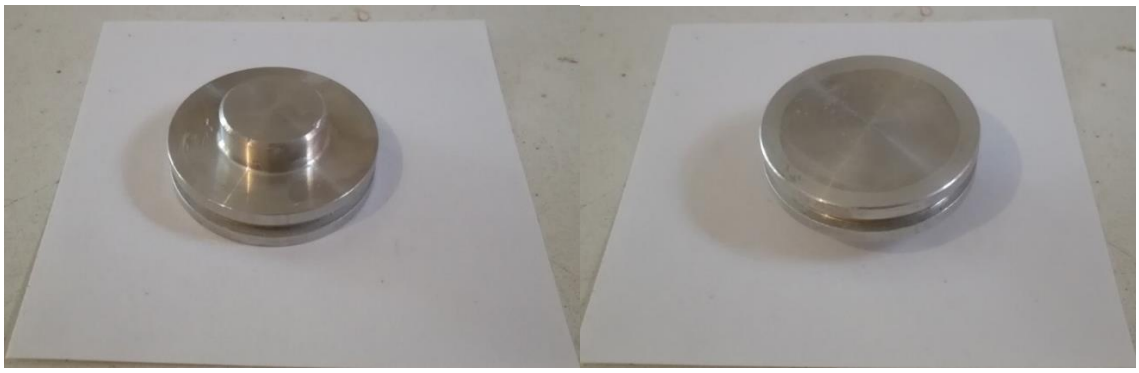

*Fig. 32 – Cover*

The aluminium cover, which was placed at the end of combustion chamber, opposite to the nozzle. Was protected from the intense heat by several layers of paper and printed plastics. Few scratches were caused by tools during assembly/disassembly.

Verdict: Nearly perfect condition, suitable for reuse.

### 3.6.1.3. Nozzle

*Fig. 33 – Nozzle*

The most stressed part of the motor, it was expected to sustain significant damage from the heat and gas particles at high velocity. Surprisingly, the nozzle survived with only cosmetic damages (dark stain at the throat section and few tiny scratches from tools used during disassembly). Even more surprisingly, there was **no measurable nozzle erosion** at all!

Verdict: Nearly perfect condition, suitable for reuse.

### 3.6.1.4. Inhibitors

*Fig 34. – Inhibitors*

These two propellant grain inhibitors made from PVC pipe were also expected to receive a lot of damage. Despite high pressure and temperature inside the combustion chamber they survived the test in a very good shape. They contained a lot of cinder, but after quick cleaning no significant damage was noticeable. However, an interesting phenomena was observed during the measurement - both inhibitors were slightly shrunk (the outer diameter of the pipe was reduced by almost half a millimetre). I assume this is the result of the extreme thermal cycle they were exposed to.

Verdict: Very good condition, however not suitable for reuse due to altered proportions.

### 3.6.1.5. Combustion chamber stopper

*Fig. 35 – Combustion chamber stopper*

This 3D-printed stopper placed at the end of the combustion chamber was the last part in direct contact with the combustion process. While the nozzle and inhibitors sustained minimal damages, the stopper on the other hand was totally devastated. While totally

burned up and partially melted, it did exactly what it was supposed to do – to keep the extreme temperature away from aluminium parts.

Interesting thing to notice is the melted spot in the middle. Its size, shape and position corresponds with the central channel of the fuel grain and it is clear, that the stress in this particular spot was massive and could possibly lead to structural failure of the motor. In fact, there even is a small hole through whole part in this place – luckily the cinder from the combustion process clogged the area soon enough and protected it from the heat and possibly even bigger damage.

Verdict: Extremely damaged, absolutely not suitable for reuse. **Design change is advised.**

### 3.6.1.6. Sealing rings

*Fig. 36 – Sealing rings*

These two rings on both ends of the motor were used to minimise the leaking of hot gases through gaps between the nozzle/cover and the aluminium casing. They did sustain little permanent deformation from the storage in assembled motor and small chunks of rubber were cut away during disassembly (sharp edges of grooves acted like scissors when parts were pulled apart).

Verdict: Small damages from the disassembly process. Reuse is not recommended.

### 3.6.1.7. Motor casing

*Fig. 37 – Motor casing*

This aluminium casing was the base part of the project, as it held everything together. After disassembly no major mechanical damage was registered, few scratches were made by tools during disassembly.

Verdict: Nearly perfect condition, suitable for reuse.

### 3.6.1.8. Distance papers

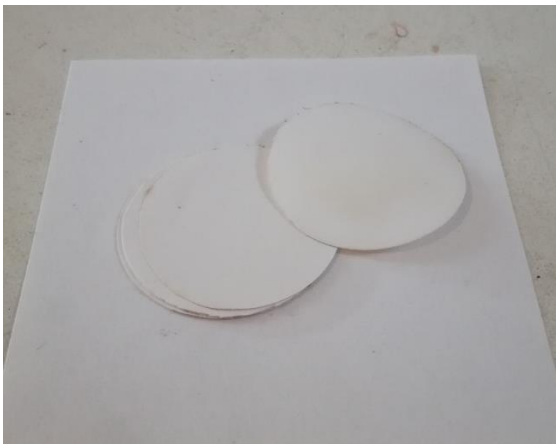

*Fig. 38 – Distance papers*

This set of circular papers was used to fill the small gap between the cover and the stopper to fix all parts in place (otherwise they would be able to travel across the casing tube). While they were in direct contact with the stopper which was destroyed by the combustion process, these papers were left completely unharmed.

Verdict: No damage taken, suitable for reuse.

## 3.7. Conclusion

Based on the results of the measurements we can say that the motor performed rather well.
Both thrust and total impulse were slightly worse than their calculated expectations, but that is understandable as those were theoretically perfect results supported with several simplifying assumptions. The burn time was significantly longer than expected, mainly due to slower burn rate of the propellant.

Considering the results reusability-wise, the motor is well suitable for repeated use. All aluminium and stainless steel parts suffered no major damage while the cost of the propellant and single-use parts is in units of USD per launch.

Speaking of reusability, the lack of nozzle erosion completely blew out my mind. Could be possibly by high quality material used in the nozzle and smaller mass flow during the burn.

## 3.8. Data summary

| | | |
|---|---|---|
| **Peak thrust** | **75** | **N** |
| **Total impulse** | **120** | **Ns** |
| **Total burn time** | **2,1** | **s** |

***Tab. 1 – Data summary***

## Nomenclature

F = force [N]

m = mass [kg]

g = standard gravitational constant [9,81 $m/s^2$]

T = temperature [K]

a = acceleration [$m/s^2$]

u; v = velocity [m/s]

$I_{sp}$ = specific impulse [s]

t = time [s]

p = pressure [Pa]

R = universal gas law constant [8314,5 J/kmol·K]

γ = isentropic expansion factor [-]

$c_p$ = specific heat of the gas at constant pressure [J/kg·K]

$c_v$ = specific heat of the gas at constant volume [J/kg·K]

D; d = diameter [mm]

L = length [mm]

n = quantity [-]

ρ = density [$kg/m^3$]

A; S = area [$m^2$]

o = perimeter [mm]

k = ratio of specific heats; safety factor [-]

r = radius [mm]

σ = normal stress [Pa]

$\tau$ = shear stress [Pa]

## Abbreviations

| | |
|---|---|
| NASA | = National Aeronautics and Space Administration |
| ESA | = European Space Agency |
| SpaceX | = Space Exploration Technologies Corporation |
| SRB | = solid rocket booster |
| RP-1 | = kerosene (rocket propellant-1; redefined petroleum-1) |
| LOX | = liquid oxygen |
| HTPB | = hydroxyl-terminated polybutadiene monomer |
| BATES | = ballistic test and evaluation system |
| ANCP | = ammonium nitrate composite propellant |
| APCP | = ammonium perchlorate composite propellant |
| PVC | = polyvinyl chloride |
| CAD | = computer aided design |
| $KNO_3$ | = potassium nitrate |
| CTU | = Czech Technical University in Prague |
| USD | = United States dollar |

**List of pictures**

# List of literature


[1] Braeunig.us. (2019). *Basics of Space Flight: Rocket Propulsion*. [online] Available at: http://www.braeunig.us/space/propuls.htm [Accessed 31 Jul. 2019].

[2] Force diagram for rocket engine thrust. (2009). [image] Available at: https://en.wikipedia.org/wiki/File:Rocket_thrust.svg [Accessed 31 May 2019].

[3] Sutton, G. and Biblarz, O. (2017). *Rocket propulsion elements*. New York: John Wiley & Sons, p.27.

[4] En.wikipedia.org. (2019). *Tsiolkovsky rocket equation*. [online] Available at: https://en.wikipedia.org/wiki/Tsiolkovsky_rocket_equation [Accessed 13 Jul. 2019].

[5] NASA's Space Shuttle Endeavour. (n.d.). [image] Available at: http://www.whoinventedthis.org/who-invented-the-space-shuttle/ [Accessed 19 Apr. 2019].

[6] Virgin Galactic's SpaceShipTwo. (n.d.). [image] Available at: https://spaceflightnow.com/2018/05/30/virgin-galactics-spaceshiptwo-completes-second-powered-test-flight/ [Accessed 27 May 2019].

[7] A de Laval nozzle, showing approximate flow velocity increasing from green to red in the direction of flow. (2005). [image] Available at: https://en.wikipedia.org/wiki/Rocket_engine_nozzle#/media/File:De_laval_nozzle.svg [Accessed 24 Jun. 2019].

[8] Nozzle de Laval diagram. (2008). [image] Available at: https://en.wikipedia.org/wiki/File:Nozzle_de_Laval_diagram.svg [Accessed 14 Apr. 2019].

[9] The four expansion regimes of a de Laval nozzle. (2009). [image] Available at: https://en.wikipedia.org/wiki/Rocket_engine#/media/File:Rocket_nozzle_expansion.svg [Accessed 5 May 2019].

[10] Propellants. (n.d.). [image] Available at: https://www.nakka-rocketry.net/th_grain.html [Accessed 18 May 2019].

[11] BATES. (n.d.). [image] Available at: https://www.nakka-rocketry.net/rnx_fin.html [Accessed 18 May 2019].

[12] Science.ksc.nasa.gov. (n.d.). *SOLID ROCKET BOOSTERS*. [online] Available at: https://science.ksc.nasa.gov/shuttle/technology/sts-newsref/srb.html [Accessed 11 Jul. 2019].

[13] Nakka, R. (n.d.). *Richard Nakka's Experimental Rocketry Site*. [online] Nakka-rocketry.net. Available at: https://www.nakka-rocketry.net/ [Accessed 21 Mar. 2019].